

Article

Na₄Yb(CO₃)₃F: A New UV Nonlinear Optical Material with a Large Second Harmonic Generation Response

Qiaoling Chen ¹, Min Luo ^{2,*}  and Chensheng Lin ²¹ School of Mathematics and Physics, Fujian University of Technology, Fuzhou 350118, China; cq1@fjut.edu.cn² Key Laboratory of Optoelectronic Materials Chemistry and Physics, Fujian Institute of Research on the Structure of Matter, Chinese Academy of Sciences, Fuzhou 350002, China; cslin@fjirsm.ac.cn

* Correspondence: lm8901@fjirsm.ac.cn; Tel.: +86-591-83750713

Received: 4 September 2018; Accepted: 27 September 2018; Published: 30 September 2018



Abstract: A new nonlinear optical crystals fluoride carbonate, Na₄Yb(CO₃)₃F, has been synthesized by mild hydrothermal method. The Na₄Yb(CO₃)₃F crystallizes in the noncentrosymmetric space group *Cc* (no. 9) with the lattice parameters *a* = 8.018(3), *b* = 15.929(5), *c* = 13.950(5) Å and $\beta = 101.425(6)^\circ$. The compound Na₄Yb(CO₃)₃F has a high density of [CO₃] groups. The structure can be described as one-dimensional [Na₅Yb(CO₃)₂F₂] chains connected by [CO₃] groups, forming an intricate three-dimensional (3D) framework. Other Na⁺ and Yb³⁺ cations are located in the cavities of 3D network. The powder second harmonic generation (SHG) measurement shows that Na₄Yb(CO₃)₃F features a large SHG response, about 4.3 times that of KH₂PO₄ (KDP), and is a phase-matchable material. In addition, its UV-Vis-NIR diffuse reflectance spectral data indicate that Na₄Yb(CO₃)₃F has a large optical gap about 4.72 eV, which corresponds to the UV cut-off edge of 263 nm.

Keywords: carbonate; nonlinear optical crystal; UV; crystal growth

1. Introduction

Nonlinear optical (NLO) crystals are of great importance for UV frequency conversion, due to the increasing demand on the applications of UV laser. Over the last few decades, the dominant research on the explorations of new UV NLO materials has been focused on the borates, resulting in finding many excellent potential UV NLO crystals [1–7]. However, it remains challenging to obtain practically useful materials possessing high NLO coefficients and wide UV transparency.

To date, although various ideas have been put forward on how to design NLO crystals with large SHG effect [8–10], the anionic group theory has achieved great success in guiding the design and synthesis of UV and deep-UV NLO. Based on the anionic group theory [11,12], there are two ways to produce large NLO effects: (1) favorable NLO-active structural units are in coparallel alignment in crystal and (2) the density of NLO-active structural units is high in crystal. In addition, according to the anionic groups theory, one can know that the favorable structural unit is the planar [BO₃]^{3−} group containing conjugated π -orbital in borates system, because the planar [BO₃]^{3−} anionic group has a moderate birefringence and a large microscopic second-order susceptibility $\beta^{(2)}$. Some successful examples include KBe₂BO₃F₂ [13], BaAlBO₃F [14], Sr₂Be₂B₂O₇ [15]. Analogously, [NO₃][−] and [CO₃]^{2−} anionic groups possessing the similar planar triangle structure with π -orbital are expected to be the good NLO-active anionic groups as well. The nitrates are not commonly considered as the NLO crystals candidates, attributing to their hydrolysis. However, most carbonates have stable physical and chemical properties. Thus, we choose [CO₃]^{2−} anionic groups as fundamental structural units to design novel UV NLO materials.

It is well known that the alkaline metal cations without unclosed d or f electrons contribute to the cut-off edge shifting to the UV region, because the d-d or f-f electronic transitions have negative influences on the optical band gap. In addition, the NLO crystals containing fluorine atoms, such as AB_4O_6F ($A = NH_4, Na, K, Rb, Cs$) [16–19], $M_2B_{10}O_{14}F_6$ ($M = Ca, Sr$) [20], MB_2O_3F ($M = Pb, Sn$) [21], will cause a crystal blue shift effect, because strong electronegativity of fluorine atom can effectively increase the energy band gap of compounds, thus resulting in short UV cut-off edge. Besides, the compounds that contain rare earth atoms often exhibit excellent optical properties, such as $Na_3Re(CO_3)_3$ ($Re = Y, Gd$) [22], $Cd_4ReO(BO_3)_3$ ($Re = Y, Gd, Lu$) [23] and $GdCa_4(BO_3)_3$ (GCOB) [24]. Guided by these principles, in order to obtain the novel UV NLO crystals, we expected to introduce alkali metal, rare earth and halogen fluorine atoms into carbonates to form complex fluoride carbonates.

Fluoride carbonates systems have been extensively studied in recent years, which has resulted in some excellent fluoride carbonates NLO materials, such as $K_4Ln_2(CO_3)_3F_4$ ($Ln = Pr, Nd, Sm, Gd, Eu$) [25], $ABCO_3F$ ($A = K, Rb, Cs; B = Ca, Sr, Ba$) [26], $Na_3Lu(CO_3)_2F_2$ [27], $K_{2.70}Pb_{5.15}(CO_3)_5F_3$ [28], $RbPbCO_3F$ [29] and $CsPbCO_3F$ [29]. In addition, it is noteworthy that large, centimeter size, single crystals of $KSrCO_3F$ had been successfully grown by a top seeded solution growth (TSSG) method [30]. $KSrCO_3F$ exhibited a laser damage threshold (LDT) over 700 MW cm^{-2} (1064 nm, 6 ns, 15 Hz), which suggested that fluoride carbonates' potential laser application. In this study, our further investigation of the alkali metal (Li, Na, K, Rb, Cs) and rare earth (La, Sc, Yb) fluoride carbonates system at subcritical hydrothermal condition resulted in the finding of a new noncentrosymmetric material $Na_4Yb(CO_3)_3F$, with a short UV cut-off edge and a large SHG effect. Herein we report the syntheses, crystal structure, and optical properties.

2. Materials and Methods

2.1. Reagents

Na_2CO_3 (99.8%), NaF (99.8%) were purchased from Sinopharm (Fuzhou, China). $Yb(NO_3)_3 \cdot 6H_2O$ (99.0%) were purchased from Jinan Camolai Trading Company (Jinan, China).

2.2. Syntheses of $Na_4Yb(CO_3)_3F$

A mixture of Na_2CO_3 (2.12 g, 0.02 mol), NaF (0.52 g, 0.012 mol), $Yb(NO_3)_3 \cdot 6H_2O$ (0.181 g, 0.004 mol), and H_2O (5.0 mL) was sealed in an autoclave equipped with a Teflon liner (23 mL) and heated at $220 \text{ }^\circ\text{C}$ for 5 days, followed by slow cooling to room temperature at a rate of $3 \text{ }^\circ\text{C/h}$. The reaction product was washed with deionized water and ethanol and then dried in air. Colorless brick-shaped $Na_4Yb(CO_3)_3F$ crystals were obtained.

2.3. Single Crystal X-ray Diffraction

Single crystal X-ray diffraction data were collected at room temperature on a Rigaku Mercury CCD diffractometer (Rigaku, Tokyo, Japan) with graphite-monochromatic Mo $K\alpha$ radiation ($\lambda = 0.71073 \text{ \AA}$). A transparent block of crystal was mounted on a glass fiber with epoxy for structure determination. A hemisphere of data was collected using a narrow-frame method with ω -scan mode. The data were integrated using the CrystalClear program, and the intensities were corrected for Lorentz polarization, air absorption, and absorption attributable to the variation in the path length through the detector faceplate. Absorption corrections based on the Multiscan technique were also applied. The structure was solved by the direct methods. Then they were refined by full-matrix least-squares fitting on F^2 by SHELX-97 [31]. All nonhydrogen atoms were refined with anisotropic thermal parameters. The structure was verified using the ADDSYM algorithm from the program PLATON [32], and no higher symmetries were found. Relevant crystallographic data and details of the experimental conditions for $Na_4Yb(CO_3)_3F$ are summarized in Table 1, atomic coordinates and isotropic displacement coefficients are listed in Table S1, and bond lengths in Table S2 in the Supplementary Information.

Table 1. Crystal data and structure refinement for Na₄Yb(CO₃)₃F.

Formula	Na ₄ Yb(CO ₃) ₃ F
Formula Mass (amu)	464.03
Crystal System	Monoclinic
Space Group	Cc
a (Å)	8.018(3)
b (Å)	15.929(5)
c (Å)	13.950(5)
β (°)	101.425(6)
V (Å ³)	1746.4(11)
Z	8
ρ (calcd) (g/cm ³)	3.530
Temperature (K)	293(2)
λ (Å)	0.71073
F (000)	1647
M (mm ⁻¹)	11.602
R/wR (I > 2σ (I))	0.0171/0.0347
R/wR (all data)	0.0177/0.0350
GOF on F ²	1.077
Absolute Structure Parameter	0.00

$$R(F) = \frac{\sum ||F_o| - |F_c||}{\sum |F_o|}, \quad wR(F_o^2) = \left[\frac{\sum w(F_o^2 - F_c^2)^2}{\sum w(F_o^2)^2} \right]^{1/2}$$

2.4. Powder X-ray Diffraction

Polycrystalline materials were ground from single crystals. X-ray diffraction patterns of polycrystalline materials were obtained on a Rigaku Dmax2500 powder X-ray diffractometer (Rigaku, Tokyo, Japan) by using Cu K α radiation ($\lambda = 1.540598 \text{ \AA}$) at room temperature in the angular range of $2\theta = 5\text{--}65^\circ$ with a scan step width of 0.05° and a fixed time of 0.2 s. The powder XRD patterns showed good agreement with the calculated XRD patterns from the single-crystal models. (Figure 1).

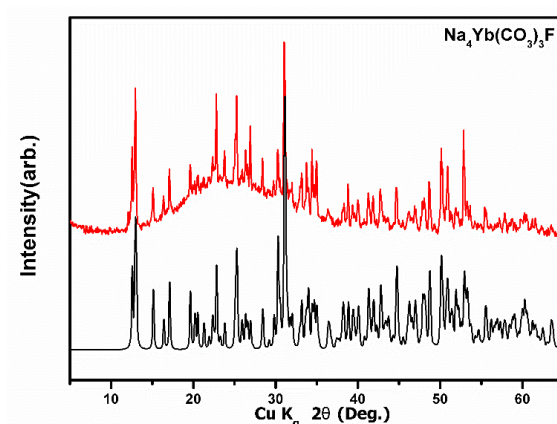


Figure 1. X-ray powder diffraction patterns of Na₄Yb(CO₃)₃F. The black curves are the calculated ones, the red are the patterns of samples.

2.5. Thermal Analysis

The TG/DTA scans were measured on a NETZSCH STA 449C (NETZSCH, Bavaria, Germany). Reference (Al₂O₃) and crystal samples (3–10 mg) were enclosed in Al₂O₃ crucibles and heated from room temperature to 900 °C at a rate of 10 °C/min under a constant flow of nitrogen gas.

2.6. UV-Vis Diffuse Reflectance Spectroscopy

UV-vis Diffuse Reflectance Spectroscopy data were recorded at room temperature using a powder sample with BaSO₄ as a standard (100% reflectance), on a PerkinElmer Lambda-900 UV/vis/NIR spectrophotometer (PerkinElmer, Berlin, Germany) and scanned at 200–2500 nm. Reflectance spectra were converted to absorbance using the Kubelka-Munk function [33,34].

2.7. Second-Harmonic Generation

Polycrystalline second-harmonic generation (SHG) signals were measured using the method adapted from Kurtz and Perry [35]. Since SHG efficiencies are known to depend strongly on particle size, polycrystalline samples were ground and sieved into the following particle size ranges: 25–45, 45–62, 62–75, 75–109, 109–150, and 150–212 μm . The samples were pressed between glass microscope cover slides and secured with tape in 1 mm thick aluminum holders containing an 8 mm diameter hole. To make relevant comparisons with known SHG materials, crystalline KDP were also ground and sieved into the same particle size ranges. The samples were then placed in a light-tight box and irradiated with a pulsed laser. The measurements were performed with a Q-switched Nd:YAG laser at 1064 nm. A cutoff filter was used to limit background flash-lamp light on the sample, and an interference filter (530 ± 10 nm) was used to select the second harmonic for detection with a photomultiplier tube attached to a RIGOL DS1052E 50-MHz oscilloscope. This procedure was then repeated using the standard nonlinear optical materials KDP, and the ratio of the second-harmonic intensity outputs was calculated. No index-matching fluid was used in any of the experiment.

2.8. Computational Methods

The first-principle calculations were performed by the plane-wave pseudopotential method implemented in the CASTEP package [36]. The ion-electron interactions were modeled by the optimized normal-conserving pseudopotentials for all constituent elements. In this model, C $2s^2 2p^2$, O $2s^2 2p^4$, Na $2s^2 2p^6 3s^1$ and Yb $4f^{14} 5s^2 5p^6 6s^2$ electrons were treated as the valence electrons, respectively. The kinetic energy cutoff of $\text{Na}_4\text{Yb}(\text{CO}_3)_3\text{F}$ was set at 850 eV. The convergence criteria of total energy for the title compounds was set at 1.0×10^{-5} eV/atom. According to the Monkhorst-Pack scheme [37], the k-point meshes in the Brillouin zone was sampled as $6 \times 3 \times 3$. Generalized gradient approximation (GGA) in the scheme of Perdew-Burke-Eruzerhof (PBE) [38] describe the exchange and correlative potential of electron-electron interactions. Both the lattice constants and atom sites were fully fixed within experimental values. For the optical property calculations, the scissors-correction method was adopted, where the scissors operator was set as the difference between the experimental and GGA-PBE bandgaps.

The “velocity-gauge” formula derived by Sipe et al. [39] was employed to calculate the SHG coefficient. The calculated second-order susceptibilities are expressed as follows:

$$\chi^{(2)}(-2\omega; \omega, \omega) = \frac{i}{2} \left| \frac{e}{m\omega} \right|^3 \sum_{ijl} \int_{\text{BZ}} \frac{dk}{4\pi^3} \frac{P_{ij} P_{jl} P_{li}}{2E - E_{ji}} \left[\frac{f_{il}}{E - E_{li}} - \frac{f_{jl}}{E - E_{jl}} \right], \quad (1)$$

where $e = h\omega$, $E_{ji} = E_j - E_i$, $f_{il} = f_i - f_l$, etc.; f_i is the Fermi occupation factor of the single-particle state i , and P_{ij} are momentum matrix elements. Subscripts i , j , and l can be thought of as labeling the band index at a given k in the BZ; quantities like P_{ij} , and E_{jk} are therefore functions of k . In this formula, the optical transition dipole moment p is taken from dielectric function of CASTEP optical properties calculation.

In this manner, we calculated the imaginary part of $\chi^{(2)'}$, and the real part of $\chi^{(2)''}$ was obtained by Kramers–Kronig Relations on the imaginary part. The total second-order susceptibility $\chi^{(2)} = \left(\left| \chi^{(2)'} \right|^2 + \left| \chi^{(2)''} \right|^2 \right)$ and $d = 2\chi^{(2)}$.

3. Results and Discussion

3.1. Crystal Structure

$\text{Na}_4\text{Yb}(\text{CO}_3)_3\text{F}$ crystallizes into a monoclinic crystal system with an acentric space group of Cc . As shown in Figure 2, its structure can be described as the $[\text{CO}_3]$ groups connect to the one-dimensional $[\text{Na}_5\text{Yb}(\text{CO}_3)_2\text{F}_2]$ chains to construct an intricate three-dimensional framework. The Na(2), Na(3),

Na(8) and Yb(1) atoms reside in the cavities of the 3D network. The Na(2), Na(8) atoms are 7-fold coordinated, respectively, forming [Na(2)O₇] and [Na(8)O₆F] polyhedra and Na(3) atoms are 6-fold coordinated, forming [Na(3)O₆] polyhedra. The other Na atoms are surrounded by five O atoms and one F atom, forming [NaO₅F] polyhedral (Figure 2c). The Yb atoms occupy two crystallographic sites and exhibit different coordination environments. The Yb(1) atom is coordinated to eight O atoms, forming [Yb(1)O₈] polyhedra, while the Yb(2) atom is coordinated to five O atoms and two F atoms forming [Yb(2)O₅F₂] polyhedral (Figure 2c). The [CO₃] groups form rods along the c-axis that can be described as piercing or cross-linking (on-edge) infinite corrugated sheets of edge sharing (Figure 2b). In terms of [CO₃] triangles, the range of C–O bond lengths is between 1.248(6) and 1.333(5) Å, and O–C–O bond angles range from 114.1(4) to 124.8(4)°. It is noteworthy that one-third of the [CO₃] groups are approximately parallel to a-b plane and in the same direction, giving main contribution to the SHG effect and the other [CO₃] groups inclined to a-b plane having additional contributions to the SHG effect.

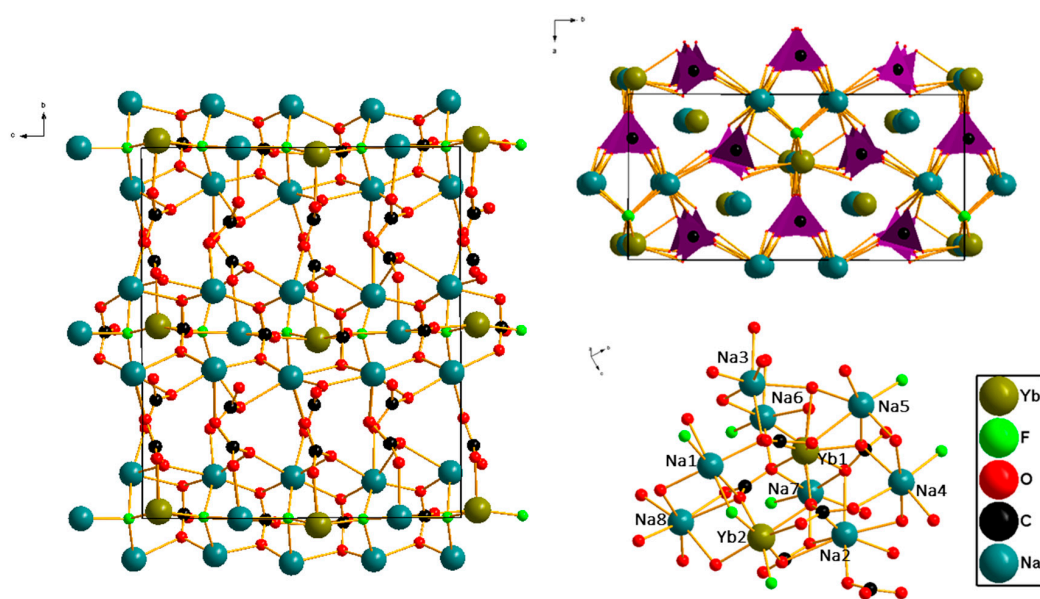


Figure 2. Crystal structure of Na₄Yb(CO₃)₃F.

3.2. Thermal Analysis

As shown in Figure 3, the thermogravimetric analysis (TGA) were performed to investigate the thermal properties of Na₄Yb(CO₃)₃F. TGA curve revealed that the compound was stable up to 300 °C. The weight loss occurred in the temperature interval about 300–500 °C, which can be ascribed to the loss (weight %) of 1.5 moles of CO₂ gas per one mole of Na₄Yb(CO₃)₃F (exp./th. = 14.7/14.2).

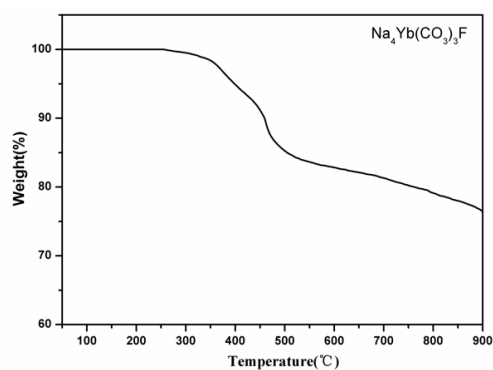


Figure 3. The thermogravimetric diagrams for Na₄Yb(CO₃)₃F.

3.3. Diffuse-Reflectance Spectroscopy

The data of UV-vis diffuse reflectance spectra collected for $\text{Na}_4\text{Yb}(\text{CO}_3)_3\text{F}$ in the region of 200–2500 nm is presented in Figure 4. Absorption (K/S) data were calculated from the following Kubelka-Munk function: $F(R) = (1 - R)^2/2R = K/S$, where R is the reflectance, K is the absorption, and S is the scattering. In the (K/S)-versus- E plots, extrapolating the linear part of the rising curve to zero provided the onset of absorption. The optical diffuse reflectance spectrum study indicated that the optical band gap for $\text{Na}_4\text{Yb}(\text{CO}_3)_3\text{F}$ was approximately 4.72 eV with UV cut-off edges of 263 nm.

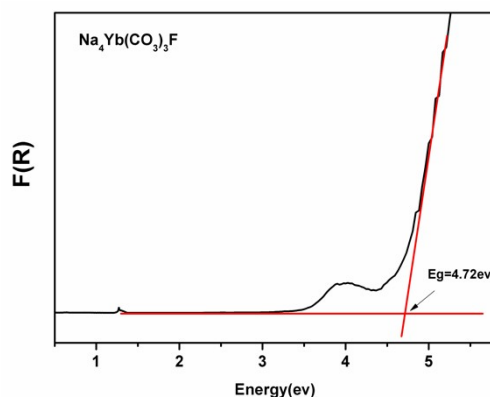


Figure 4. Optical diffuse reflectance spectra for $\text{Na}_4\text{Yb}(\text{CO}_3)_3\text{F}$.

3.4. NLO Properties

The curves of the SHG signals, as a function of particle size from the measurements made on ground crystals of $\text{Na}_4\text{Yb}(\text{CO}_3)_3\text{F}$, were shown in Figure 5. According to the rule proposed by Kurtz and Perry, the titled compound was phase-matching in the visible region. The KDP sample was used as a reference. The measurement of second-harmonic signal for $\text{Na}_4\text{Yb}(\text{CO}_3)_3\text{F}$ was found to be about $4.3 \times$ KDP. Since the reported d_{36} coefficient for KDP was 0.39 pm/V, the derived d_{eff} coefficients for $\text{Na}_4\text{Yb}(\text{CO}_3)_3\text{F}$ was 1.28 pm/V.

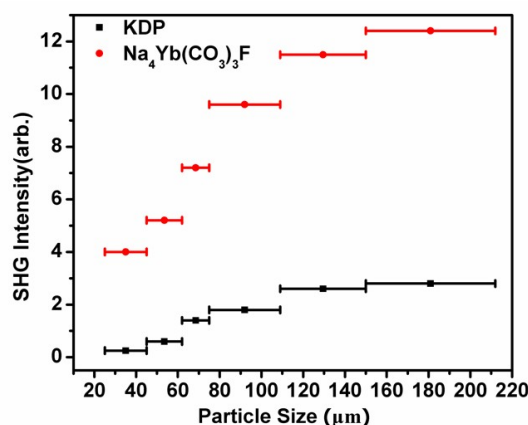


Figure 5. SHG measurements of $\text{Na}_4\text{Yb}(\text{CO}_3)_3\text{F}$ ground crystals (red circle) with KDP (black square) as a reference.

In order to study the relationship between structure and NLO properties, the computational method based on the anionic group theory reported in reference [40] was employed. The detailed computational processes are presented in the Supplementary Information, and the calculated results can be seen in Tables S3 and S4. According to Equations (2) and (4) in the Supplementary Information, without considering localized field (F), the NLO coefficient $\chi^{(2)}_{ijk}$ depended on two factors: (1) the structural criterion (C) and (2) the density of $[\text{CO}_3]$ group (n/V). The C factor was between 0 to 1,

representing the average result of the addition of the anionic group dipole vectors in the unit cell. That is, the C factor directly reflected the arrangement of anionic groups in the cell. For $\text{Na}_4\text{Yb}(\text{CO}_3)_3\text{F}$, the calculated value of C factor was 0.86 approaching 1. The result indicated that all $[\text{CO}_3]$ groups were approximately in coparallel alignment, giving a great contribution to macroscopic NLO coefficients. In addition, apart from large C value, compound $\text{Na}_4\text{Yb}(\text{CO}_3)_3\text{F}$ had a high density of $[\text{CO}_3]$ groups (0.0137), which was larger than those of some known carbonate NLO crystals, such as KSrCO_3F (0.0089) and $\text{Na}_3\text{Lu}(\text{CO}_3)_2\text{F}_2$ (0.0117). Therefore, a large C factor and the high density of $[\text{CO}_3]$ group (n/V) resulted in large SHG effect of $\text{Na}_4\text{Yb}(\text{CO}_3)_3\text{F}$.

3.5. Theoretical Calculations

For a deeper understanding of the bonding interactions in $\text{Na}_4\text{Yb}(\text{CO}_3)_3\text{F}$, theoretical calculations were adopted based on DFT methods. The calculated band structure is presented in Figure 6. Compound $\text{Na}_4\text{Yb}(\text{CO}_3)_3\text{F}$ exhibited a direct band gap of 4.573 eV at Γ point. This value was smaller than the experimental values, due to the underestimation of band gap by DFT method. The total and partial densities of states (DOS and PDOS) are presented in Figure 7, in which the occupied part of the valence band can be subdivided into three regions, separated by energy gaps. The valence bands (VB) in the lowest region, ranging from -24.0 eV to -20.0 eV, were mainly occupied by p orbitals of Yb and Na atom and s orbitals of C, O and F atom, while those from -20 eV to -17.0 eV have most of the contributions from O- $2s$ and C- $2p$. In the vicinity of the Fermi level, namely, from -9.0 eV to 0 eV in the VB, O- $2p$, and C- $2p$ orbitals were predominantly involved and overlap fully, revealing that the strong covalent interactions of C–O bonds. In the range from 4.6 eV to 8.0 eV in the conduction band (CB), C- $2p$, O- $2p$ and Yb- $4f$ state were mainly occupied. Notably, since the VB maximum and the CB minimum were mainly composed of the O $2p$ and C $2p$ orbitals, respectively, this indicated that the electron transition was mainly contributed to by inside excitation of the $[\text{CO}_3]^{2-}$ group. Therefore, the SHG coefficients primarily originate from the contribution of CO_3 .

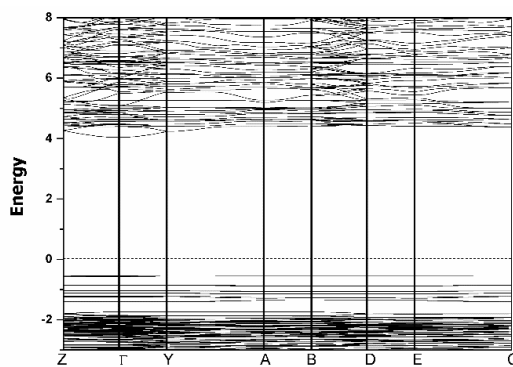


Figure 6. The calculated band structure of $\text{Na}_4\text{Yb}(\text{CO}_3)_3\text{F}$.

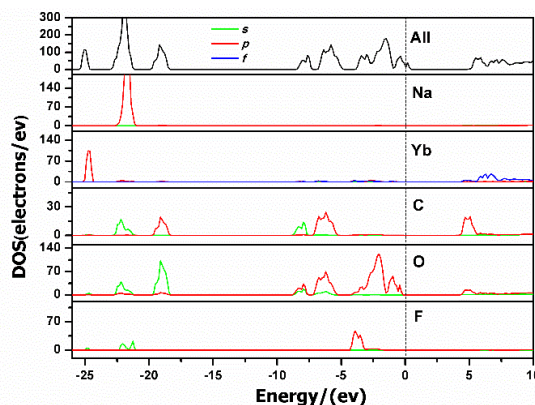


Figure 7. Total and partial densities of states for $\text{Na}_4\text{Yb}(\text{CO}_3)_3\text{F}$.

To gain theoretical values of the SHG coefficients, the “velocity-gauge” formula derived by Sipe et al. was used. Since the space group of the title compound belonged to class *m*, there were 10 nonvanishing tensors of second-order susceptibility. Under the restriction of Kleinman’s symmetry, only six independent SHG tensor components (d_{11} , d_{12} , d_{13} , d_{15} , d_{24} , and d_{33}) were considered. The calculated six frequency dependent NLO components (d_{11} , d_{12} , d_{13} , d_{15} , d_{24} , and d_{33}) were plotted in Figure 8. The calculated largest tensor at a wavelength of 1064 nm (1.165 eV) is d_{11} and the value of d_{11} is 0.90 pm/V, which are close to the experimental one.

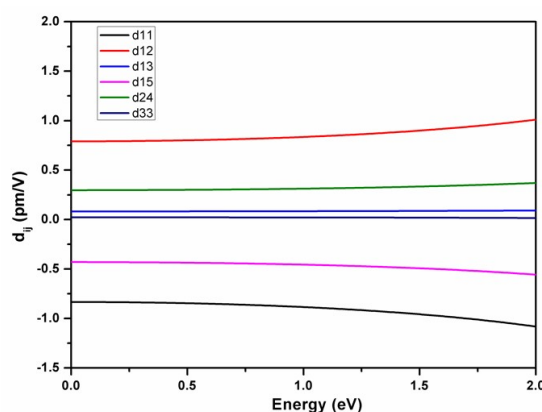


Figure 8. Calculated frequency-dependent second harmonic generation coefficients for $\text{Na}_4\text{Yb}(\text{CO}_3)_3\text{F}$.

4. Conclusions

In summary, we have synthesized a novel ultraviolet nonlinear-optical material $\text{Na}_4\text{Yb}(\text{CO}_3)_3\text{F}$ under a subcritical hydrothermal condition. The powder SHG test shows that the compound exhibits a large SHG response about 4.3 times KH_2PO_4 (KDP). In addition, the result from the UV-vis diffuse reflectance spectroscopy study of the powder sample indicates that the short-wavelength absorption edge of $\text{Na}_4\text{Yb}(\text{CO}_3)_3\text{F}$ is about 263 nm. The features of a short UV cutoff edge and a large SHG effect are favorable in practical applications as UV NLO materials.

Supplementary Materials: The following are available online at <http://www.mdpi.com/2073-4352/8/10/381/s1>, Table S1: Atomic coordinates and equivalent isotropic displacement parameters. $U(\text{eq})$ is defined as one third of the trace of the orthogonalized U_{ij} tensor. Table S2: Bond lengths (\AA) for $\text{Na}_4\text{Yb}(\text{CO}_3)_3\text{F}$. Table S3: The values of geometrical factor. Table S4: NLO effects of $\text{Na}_4\text{Yb}(\text{CO}_3)_3\text{F}$.

Author Contributions: Q.C. carried out experimental work (synthesis, crystallization and characterization) and wrote the manuscript. C.L. performed theoretical calculations. M.L. conceived and designed this study.

Funding: This research was supported by the National Natural Science Foundation of China (Grant Nos. 51425205, U1605245, 51602309), the National Key Research and Development Plan of Ministry of Science and Technology (Grant No. 2016YFB0402104) and the Strategic Priority Research Program of the Chinese Academy of Sciences (Grant No. XDB20000000).

Conflicts of Interest: The authors declare no conflict of interest.

References

1. Luo, M.; Song, Y.; Liang, F.; Ye, N.; Lin, Z. $\text{Pb}_2\text{BO}_3\text{Br}$: A novel nonlinear optical lead borate bromine with a kbbf-type structure exhibiting strong nonlinear optical response. *Inorg. Chem. Front.* **2018**, *5*, 916–921. [[CrossRef](#)]
2. Zou, G.; Lin, C.; Jo, H.; Nam, G.; You, T.-S.; Ok, K.M. $\text{Pb}_2\text{BO}_3\text{Cl}$: A tailor-made polar lead borate chloride with very strong second harmonic generation. *Angew. Chem. Int. Ed.* **2016**, *55*, 12078–12082. [[CrossRef](#)] [[PubMed](#)]
3. Tran, T.T.; Koocher, N.Z.; Rondinelli, J.M.; Halasyamani, P.S. Beryllium-free $\beta\text{-Rb}_2\text{Al}_2\text{B}_2\text{O}_7$ as a possible deep-ultraviolet nonlinear optical material replacement for $\text{KBe}_2\text{BO}_3\text{F}_2$. *Angew. Chem. Int. Ed.* **2017**, *56*, 2969–2973. [[CrossRef](#)] [[PubMed](#)]

4. Song, Y.; Luo, M.; Liang, F.; Lin, C.; Ye, N.; Yan, G.; Lin, Z. Experimental and ab initio studies of $\text{Cd}_5(\text{BO}_3)_3\text{Cl}$: The first cadmium borate chlorine nlo material with isolated BO_3 groups. *Dalton Trans.* **2017**, *46*, 15228–15234. [[CrossRef](#)] [[PubMed](#)]
5. Zhao, S.; Kang, L.; Shen, Y.; Wang, X.; Asghar, M.A.; Lin, Z.; Xu, Y.; Zeng, S.; Hong, M.; Luo, J. Designing a beryllium-free deep-ultraviolet nonlinear optical material without a structural instability problem. *J. Am. Chem. Soc.* **2016**, *138*, 2961–2964. [[CrossRef](#)] [[PubMed](#)]
6. Yu, N.; Wang, S.C.; Ye, N.; Liang, F.; Lin, Z.S.; Luo, M.; Poeppelmeier, K.R. A deep-ultraviolet nonlinear optical crystal: A strontium beryllium borate fluoride with planar $\text{Be}(\text{O}/\text{F})_3$ groups. *Chem. Mater.* **2016**, *28*, 4563–4571. [[CrossRef](#)]
7. Guo, S.; Jiang, X.; Liu, L.; Xia, M.; Fang, Z.; Wang, X.; Lin, Z.; Chen, C. $\text{BaBe}_2\text{BO}_3\text{F}_3$: A kbbf-type deep-ultraviolet nonlinear optical material with reinforced $[\text{Be}_2\text{BO}_3\text{F}_2]_\infty$ layers and short phase-matching wavelength. *Chem. Mater.* **2016**, *28*, 8871–8875. [[CrossRef](#)]
8. Young, J.; Lalkiya, P.; Rondinelli, J.M. Design of noncentrosymmetric perovskites from centric and acentric basic building units. *J. Mater. Chem. C* **2016**, *4*, 4016–4027. [[CrossRef](#)]
9. Cammarata, A.; Zhang, W.; Halasyamani, P.S.; Rondinelli, J.M. Microscopic origins of optical second harmonic generation in noncentrosymmetric–nonpolar materials. *Chem. Mater.* **2014**, *26*, 5773–5781. [[CrossRef](#)]
10. Cammarata, A.; Rondinelli, J.M. Contributions of correlated acentric atomic displacements to the nonlinear second harmonic generation and response. *ACS Photonics* **2014**, *1*, 96–100. [[CrossRef](#)]
11. Chen, C.; Wu, Y.; Li, R. The anionic group theory of the non-linear optical effect and its applications in the development of new high-quality nlo crystals in the borate series. *Int. Rev. Phys. Chem.* **1989**, *8*, 65–91. [[CrossRef](#)]
12. Chen, C.T.; Liu, G.Z. Recent advances in nonlinear optical and electro-optical materials. *Annu. Rev. Mater. Res.* **1986**, *16*, 203–243. [[CrossRef](#)]
13. Mei, L.; Huang, X.; Wang, Y.; Wu, Q.; Wu, B.; Chen, C. Crystal-structure of $\text{KBe}_2\text{BO}_3\text{F}_2$. *Z. Kristallogr.* **1995**, *210*, 93–95. [[CrossRef](#)]
14. Hu, Z.G.; Yoshimura, M.; Muramatsu, K.; Mori, Y.; Sasaki, T. A new nonlinear optical crystal- $\text{BaAlBO}_3\text{F}_2$ (BABF). *Jpn. J. Appl. Phys.* **2002**, *41*, L1131. [[CrossRef](#)]
15. Chen, C.T.; Wang, Y.B.; Wu, B.C.; Wu, K.C.; Zeng, W.L.; Yu, L.H. Design and synthesis of an ultraviolet-transparent nonlinear-optical crystal $\text{Sr}_2\text{Be}_2\text{B}_2\text{O}_7$. *Nature* **1995**, *373*, 322–324. [[CrossRef](#)]
16. Wang, X.; Wang, Y.; Zhang, B.; Zhang, F.; Yang, Z.; Pan, S. $\text{CsB}_4\text{O}_6\text{F}$: A congruent-melting deep-ultraviolet nonlinear optical material by combining superior functional units. *Angew. Chem. Int. Ed.* **2017**, *129*, 14307–14311. [[CrossRef](#)]
17. Shi, G.; Wang, Y.; Zhang, F.; Zhang, B.; Yang, Z.; Hou, X.; Pan, S.; Poeppelmeier, K.R. Finding the next deep-ultraviolet nonlinear optical material: $\text{NH}_4\text{B}_4\text{O}_6\text{F}$. *J. Am. Chem. Soc.* **2017**, *139*, 10645–10648. [[CrossRef](#)] [[PubMed](#)]
18. Zhang, Z.; Wang, Y.; Zhang, B.; Yang, Z.; Pan, S. Polar fluorooxoborate, nab4o6f : A promising material for ionic conduction and nonlinear optics. *Angew. Chem. Int. Ed.* **2018**, *130*, 6687–6691. [[CrossRef](#)]
19. Wang, Y.; Zhang, B.; Yang, Z.; Pan, S. Cation-tuned synthesis of fluorooxoborates: Towards optimal deep-ultraviolet nonlinear optical materials. *Angew. Chem. Int. Ed.* **2018**, *57*, 2150–2154. [[CrossRef](#)] [[PubMed](#)]
20. Luo, M.; Liang, F.; Song, Y.; Zhao, D.; Xu, F.; Ye, N.; Lin, Z. $\text{M}_2\text{B}_{10}\text{O}_{14}\text{F}_6$ (M = Ca, Sr): Two noncentrosymmetric alkaline earth fluorooxoborates as promising next-generation deep-ultraviolet nonlinear optical materials. *J. Am. Chem. Soc.* **2018**, *140*, 3884–3887. [[CrossRef](#)] [[PubMed](#)]
21. Luo, M.; Liang, F.; Song, Y.; Zhao, D.; Ye, N.; Lin, Z. Rational design of the first lead/tin fluorooxoborates $\text{MB}_2\text{O}_3\text{F}_2$ (M = Pb, Sn), containing flexible two-dimensional $[\text{B}_6\text{O}_{12}\text{F}_6]_\infty$ single layers with widely divergent second harmonic generation effects. *J. Am. Chem. Soc.* **2018**, *140*, 6814–6817. [[CrossRef](#)] [[PubMed](#)]
22. Luo, M.; Lin, C.; Zou, G.; Ye, N.; Cheng, W. Sodium–rare earth carbonates with shorite structure and large second harmonic generation response. *CrystEngComm* **2014**, *16*, 4414–4421. [[CrossRef](#)]
23. Zou, G.; Ma, Z.; Wu, K.; Ye, N. Cadmium-rare earth oxyborates $\text{Cd}_4\text{ReO}(\text{BO}_3)_3$ (Re = Y, Gd, Lu): Congruently melting compounds with large shg responses. *J. Mater. Chem.* **2012**, *22*, 19911–19918. [[CrossRef](#)]

24. Aka, G.; Kahn-Harari, A.; Mougel, F.; Vivien, D.; Salin, F.; Coquelin, P.; Colin, P.; Pelenc, D.; Damelet, J.P. Linear and nonlinear-optical properties of a new gadolinium calcium oxo-borate crystal, $\text{Ca}_4\text{GdO}(\text{BO}_3)_3$. *J. Opt. Soc. Am. B* **1997**, *14*, 2238–2247. [[CrossRef](#)]
25. Mercier, N.; Leblanc, M.; Durand, J. New frequency doubling compounds $\text{K}_4\text{Ln}_2(\text{CO}_3)_3\text{F}_4$ (Ln = Pr, Nd, Sm, Gd, Eu); crystal structure and Characterization. *Eur. J. Solid State Inorg. Chem.* **1997**, *34*, 241–249. [[CrossRef](#)]
26. Zou, G.; Ye, N.; Huang, L.; Lin, X. Alkaline-alkaline earth fluoride carbonate crystals ABCO_3F (A = K, Rb, Cs; b = Ca, Sr, Ba) as nonlinear optical materials. *J. Am. Chem. Soc.* **2011**, *133*, 20001–20007. [[CrossRef](#)] [[PubMed](#)]
27. Luo, M.; Ye, N.; Zou, G.; Lin, C.; Cheng, W. $\text{Na}_8\text{Lu}_2(\text{CO}_3)_6\text{F}_2$ and $\text{Na}_3\text{Lu}(\text{CO}_3)_2\text{F}_2$: Rare earth fluoride carbonates as deep-uv nonlinear optical materials. *Chem. Mater.* **2013**, *25*, 3147–3153. [[CrossRef](#)]
28. Tran, T.T.; Halasyamani, P.S. New fluoride carbonates: Centrosymmetric $\text{KPb}_2(\text{CO}_3)_2\text{F}$ and noncentrosymmetric $\text{K}_{2.70}\text{Pb}_{5.15}(\text{CO}_3)_5\text{F}_3$. *Inorg. Chem.* **2013**, *52*, 2466–2473. [[CrossRef](#)] [[PubMed](#)]
29. Tran, T.T.; Halasyamani, P.S.; Rondinelli, J.M. Role of acentric displacements on the crystal structure and second-harmonic generating properties of RbPbCO_3F and CsPbCO_3F . *Inorg. Chem.* **2014**, *53*, 6241–6251. [[CrossRef](#)] [[PubMed](#)]
30. Zhang, W.; Halasyamani, P.S. Crystal growth and optical properties of a UV nonlinear optical material KSrCO_3F . *Crystengcomm* **2017**, *19*, 4742–4748. [[CrossRef](#)]
31. Sheldrick, G. A short history of shelx. *Acta Crystallogr. A* **2008**, *64*, 112–122. [[CrossRef](#)] [[PubMed](#)]
32. Spek, A.L. Single-crystal structure validation with the program platon. *J. Appl. Crystallogr.* **2003**, *36*, 7. [[CrossRef](#)]
33. Kubelka, P.; Munk, F. Ein Beitrag zur Optik der Farbanstriche. *Z. Tech. Phys.* **1931**, *12*, 593–601.
34. Tauc, J. Absorption edge and internal electric fields in amorphous semiconductors. *Mater. Res. Bull.* **1970**, *5*, 721–729. [[CrossRef](#)]
35. Kurtz, S.K.; Perry, T.T. Powder technique for the evaluation of nonlinear optical materials. *J. Appl. Phys.* **1968**, *39*, 3798–3813. [[CrossRef](#)]
36. Clark, S.J.; Segall, M.D.; Pickard, C.J.; Hasnip, P.J.; Probert, M.J.; Refson, K.; Payne, M.C. First principles methods using CASTEP. *Z. Kristallogr. Cryst. Mater.* **2005**, *220*, 567. [[CrossRef](#)]
37. Monkhorst, H.J.; Pack, J.D. Special points for Brillouin-zone integrations. *Phys. Rev. B* **1976**, *13*, 5188. [[CrossRef](#)]
38. Perdew, J.P.; Burke, K.; Ernzerhof, M. Generalized gradient approximation made simple. *Phys. Rev. Lett.* **1996**, *77*, 3865–3868. [[CrossRef](#)] [[PubMed](#)]
39. Ghahramani, E.; Moss, D.J.; Sipe, J.E. Full-band-structure calculation of second-harmonic generation in odd-period strained (Si)N(Ge)N/Si superlattices. *Phys. Rev. B* **1991**, *43*, 8990–9002. [[CrossRef](#)]
40. Ye, N.; Chen, Q.X.; Wu, B.C.; Chen, C.T. Searching for new nonlinear optical materials on the basis of the anionic group theory. *J. Appl. Phys.* **1998**, *84*, 555. [[CrossRef](#)]

